Journal of Biological Physics – (preprint version, see www.springerlink.com for final version)

Robert Clewley

Inferring and quantifying the role of an intrinsic current in a mechanism for a half-center bursting oscillation

A dominant scale and hybrid dynamical systems analysis

Accepted: February 2011

Abstract This paper illustrates an informatic technique for inferring and quantifying the dynamic role of a single intrinsic current in a mechanism of neural bursting activity. We analyze the patterns of the most dominant currents in a model of half-center oscillation in the leech heartbeat central pattern generator. We find that the patterns of dominance change substantially over a cycle, allowing different local reductions to be applied to the model. The result is a hybrid dynamical systems model, which is a piecewise representation of the mechanism combining multiple vector fields and discrete state changes. The simulation of such a model tests explicit hypotheses about the mechanism, and is a novel way to retain both mathematical clarity and scientific detail in answering mechanistic questions about a complex model. Several insights into the central mechanism of "escape-release" in the model are elucidated by this analysis and compared to previous studies. The broader application and extension of this technique is also discussed.

Keywords Dominant scale analysis · Hybrid dynamical systems reduction · Bursting dynamics · Model inference · Neuroinformatics · Central pattern generation

1 Introduction

Biophysical models of neural bursting activity in small circuits known as central pattern generators (CPGs) are commonly used to hypothesize rhythmogenic mechanisms behind locomotor or autonomic control [7, 12, 16]. We will study one aspect of an existing model of the leech heartbeat elemental half-center oscillator (HCO), which is part of the heartbeat CPG circuit consisting of two reciprocally-coupled neurons that burst alternately [8, 14].

Models of small neural circuits are already sufficiently high dimensional and nonlinear that they present great challenges to existing mathematical analysis tools, and typically the functional understanding of the circuits involves reductions to simpler models of some kind (e.g., see [10]). As models become more sophisticated there is an increasing demand for tools that aid in the development and clear understanding of a model's function. Simulation capabilities for large, detailed models are currently far in advance of our analytical methods for deeply understanding their function [15, 17]. Our primary aim here is to promote a formalized, hypothesis-driven modeling technique that may be able to redress the balance. In essence, this works by exploring parsimonious, abstracted descriptions of a mechanism as a form of "reverse engineering" of the full-dimensional dynamics.

Supported by NSF CISE/CCF-0829742

R. Clewley
Neuroscience Institute and
Dept. of Mathematics and Statistics
Georgia State University
Atlanta, GA 30303, USA
E-mail: rclewley@gsu.edu

We apply a "dominant scale" analysis of a central mechanism behind the heartbeat CPG oscillations [4]. This analysis decomposes a single, high-dimensional vector field to a piecewise low-dimensional reduction known as a "hybrid dynamical system" [26]. In such a system, smooth vector fields governing the dynamics of the system in different regimes are switched at discrete times indicated by zero-crossing transition events, at which point a discrete mapping may be applied to the system's state before initializing the next vector field. In contrast to making globally valid assumptions about the dynamics in order to reduce a complex model to a single reduced model, a dominant scale analysis facilitates multiple, local reductions. These are typically of lower order than a single, global reduction, and yet can also capture more details of the dynamics [5]. This approach dissects functional relationships between parameters, variables, and model behaviors at a finer granularity than is possible with traditional model manipulations.

As with any form of reverse engineering, the user must provide some initial assumptions and hypotheses about the mechanisms based on initial observations of the system [1]. This work does not focus on how a user can generate such information in a purely objective or optimal fashion, and mostly concentrates on the technique to synthesize mechanistic hypotheses into hybrid dynamical models in order to evaluate them. Indeed, iteration is a central aspect of a reverse engineering methodology, which should validate or falsify the initial hypotheses and lead to a more refined and robust description that can be tested further. The proposed methodology is not intended as a standalone replacement of all subjective analytical steps with objective ones. Instead, it attempts to assist a human user in performing a logical, and sometimes qualitative, analysis of complex dynamics, with greater confidence and resolution.

We will restrict ourselves to a simple case study involving a single intrinsic current of the leech heartbeat CPG model, namely the hyperpolarization-activated current I_h. We do this for the purposes of exposition, despite the presence of several functionally relevant currents to explore in this CPG. Nonetheless, we will uncover some novel insights into the role of this current in this CPG as well as verify previously established insights by our method. Motivated by some broad numerical observations, initial mechanistic hypotheses are presented in Section 4, but their precise choices are not critical to this work. First of all, the iterative nature of the methodology is such that bad choices should rapidly become apparent during testing. There is naturally more ambiguity in the other choices. However, a key aspect of the methodology is use of concrete means to evaluate a reduced model ("metrics") that are suited to the resolution of investigation. On further iteration of the reverse engineering process, more subtle questions may be posed, for which both the metrics and the reduced model decomposition can be refined accordingly. We will suggest future directions of this kind based on the initial findings for this case study demonstration without pursuing them here.

1.1 Leech heartbeat case study

Previous studies of this HCO model and electrophysiological studies of the leech heartbeat have addressed fundamental questions about the mechanism of bursting [8, 14, 18–20, 24, 25]. Regarding I_h specifically, these questions can be summarized in terms of roles:

R1: What role does I_h have in the existence of a stable HCO rhythm?
R2: What role does I_h have in the modulation of the rhythm?

To these we add two questions, which investigate I_h more thoroughly:

R3: What role does I_h have in the robustness of the rhythm?
R4: What role do the details of activation / deactivation dynamics of I_h have in the performance of the rhythm?

The primary manipulation of I_h in previous modeling studies was to adjust its maximum conductance $\bar{g}_\mathrm{h}$, including setting it to zero to remove the effect of the current altogether. In conjunction with manipulations of other currents, this approach has facilitated natural language descriptions of the mechanistic role of I_h. The maximal conductance is a physiologically relevant parameter to vary, but this work dissects the dynamics in a different way. We keep $\bar{g}_\mathrm{h}$ at its canonical value from Hill et al. [14], and infer from the behavior of the model that there are different "regimes" during one oscillation of the HCO in which different currents dominate. From this we hypothesize different roles for I_h in each regime, and explore the replacement of I_h in one cell of the HCO with a simple but functionally equivalent behavior for each regime. We will reduce only one neuron of the coupled pair, in a similar fashion to the neural-silicon circuit of Sorensen et al. [24]. The purpose of this is to use the unreduced neuron as a reference, so that the quality of a reduction in the other neuron can be measured by the degree of symmetry preservation in the coupled system.

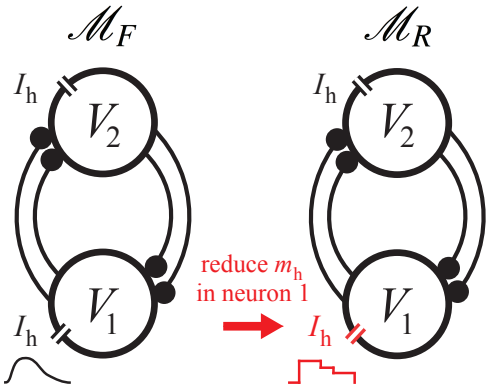

Fig. 1 The half-center oscillator model for the leech heartbeat central pattern generator, showing the two forms of reciprocal inhibitory synaptic coupling present in the circuit ("graded" and "spike-mediated"), and the intrinsic current of focus for the analysis: the hyperpolarization activated current I_h. On the left is the full 19-dimensional model $\mathscr{M}_F$. On the right, the reduced "hybrid dynamical systems" model $\mathscr{M}_R$ utilizes a piecewise constant reduced form for the activation m_h in I_h, applied only to neuron 1.

Functional criteria on the behavior of the HCO model are required to characterize the role of I_h in the CPG rhythm. We will use five functional metrics: cycle period, relative cycle phase between the two cells ("phase symmetry"), duty cycle, inter-spike interval (ISI), and phase response properties of the circuit to weak perturbations. Previous modeling studies of this model have not considered the phase response properties in detail. The metrics will be investigated over a range of maximal synaptic conductances $\bar{g}_{\mathrm{SynS}}$ for the spike-mediated coupling, which is a physiologically important parameter used in previous computational studies of this circuit [20]. We will then make a comparison of these metrics between the original HCO model and the reduced form.

We briefly review the HCO model in Section 2. In Section 3 we make broad and informal observations in relation to previous work, based on measurements of time scales and the comparison of the current terms in the model that control the motion of the membrane potentials. From these observations, explicit hypotheses are developed into a hybrid dynamical model in Section 4, which are tested in Section 5 and discussed in Section 6.

2 The HCO model

Each interneuron in the leech heartbeat HCO model consists of a single somatic compartment with membrane potential V, whose rate of change is determined by a current balance equation made up of several intrinsic ion channel currents and two forms of inhibitory synaptic input current originating from the other neuron. It is illustrated in Figure 1. The existing, "full" version of the model will be denoted $\mathscr{M}_F$ and has been developed over several studies. The version of the equations and parameters used here is described fully in [8], based on the model of Hill et al. [14]. The form of the ordinary differential equation (ODE) for V is

$$C\dot{V} = -\sum I_{\mathrm{ionic}} - I_{\mathrm{applied}} - I_{\mathrm{syn}}, \tag{1}$$

for a membrane capacitance $C = 0.5$nF, a sum of ionic currents and an applied current (which is zero unless otherwise stated). Throughout this paper, the units of V are volts, those of current are pA, and those of conductance are nS. In using the Hodgkin-Huxley formalism, each intrinsic ionic current takes the form $I = \bar{g}m^p h^q (V - E)$ for channel reversal potential E, maximum conductance $\bar{g}$, activation gating variable m and, if present, inactivation gating variable h, for some non-negative integer powers p and q. The kinetics of each gating variable are governed by a first-order differential equation. The model contains a passive leak current $I_L = \bar{g}_L (V - E_L)$ and 8 active ionic currents: a fast Na^+ current (with activation m_{Na} and inactivation h_{Na}), three types of K^+ current (m_{K1}, h_{K1}; m_{K2}, h_{K2}; and m_{KA}), a persistent Na^+ current (m_P), a hyperpolarization-activated current (m_h), and a rapidly and slowly inactivating low-threshold Ca^{2+} current (m_{CaF}, h_{CaF}; m_{CaS}, h_{CaS}).

Because we focus on I_h, we detail its definition further: $I_h = \bar{g}_h m_h^2 (V - E_h)$, where $\bar{g}_h = 4.0$nS and $E_h = -0.021$V. The activation is governed by $\dot{m}_h = (m_{h,\infty} - m_h)/\tau_h$. The time scale and steady state activation

functions are given by

$$\tau_{\rm h}(V) = 0.7 + \frac{1.7}{1+e^{-100(V+0.073)}} \text{ and } m_{\rm h,\infty}(V) = \frac{1}{1+2e^{180(V+0.047)}+e^{500(V+0.047)}}.$$

The cells are reciprocally inhibited by both slow-acting "graded" (G) and fast-acting "spike-mediated" (S) forms of synaptic inhibition [18]. The synaptic current models use a total of 5 variables but $I_{\rm SynG}$ and $I_{\rm SynS}$ appear in Eq. (1) according to

$$I_{\rm SynG} = \bar{g}_{\rm SynG}\frac{P^3}{Co+P^3}\left(V-E_{\rm Syn}\right), \quad I_{\rm SynS} = \bar{g}_{\rm SynS}MY\left(V-E_{\rm Syn}\right),$$

where P, M, and Y are three of the synaptic variables, $E_{\rm Syn} = -0.0625$V, $\bar{g}_{\rm SynG} = 30$nS, $\bar{g}_{\rm SynS} = 150$nS, and $Co = 1\times10^{-32}$ is constant. With the 5 synaptic variables there are a total of 19 dynamic variables per neuron in model $\mathscr{M}_F$. The remaining details of the currents are not important to the analysis undertaken here.

3 Preparatory observations

Busting activity in this CPG is most fundamentally split into the "active" or "bursting" state (hereon denoted B) in which the cell generates action potential spikes, and the "recovery" or "inhibited" state (hereon denoted I). Previous work has identified that $I_{\rm h}$ is important for an "escape"-based mechanism underlying the creation of a rhythmic cycle in the HCO, and for determining its period [14]. Briefly, the mechanism works as follows. A neuron inhibited by its partner in the HCO is in the inhibited state I. Eventually, it pro-actively overcomes the inhibition, spikes again itself, and thereby stops its partner from continuing its burst of spikes. $I_{\rm h}$ acts to depolarize the neuron from I into B due to $E_{\rm h}$ being more depolarized than the threshold for action potentials. $I_{\rm h}$ appears to play a major role in balancing the hyperpolarizing effect of $I_{\rm L}$ (for which $E_{\rm L} = -0.0635$) and ultimately overcomes the effect of $I_{\rm SynS}$ caused by action potential spikes arriving from the neuron in B. As noted in previous studies, the situation is more complex, and there are aspects present of a "release"-based mechanism, primarily involving the decay of $I_{\rm CaS}$.

Through analysis of $\mathscr{M}_F$ we now focus on which currents dominate the activity of the membrane potential V_1 of neuron 1 during I. The dynamics of the membrane potentials lie within a high conductance regime because $\tau_V = C/\sum_i \bar{g}_i m_i^{p_i} h_i^{q_i}$, the effective time constant for the membrane, stays small throughout each cycle [22]. We will not focus on the role of $I_{\rm h}$ at the resolution of dynamics within single spikes, and at slower time scales in the cycle τ_V remains within a range of 0.02–0.03s on average, over both B and I. It is therefore appropriate to this study to use the type of dominant scale analysis performed on bursting cells in a crustacean stomatogastric system by comparing the changing magnitudes of the currents over a cycle [5]. (In a purely high-conductance regime this provides equivalent information to studying the "influence" sensitivity quantities also considered in [4,5].)

Over one cycle, $m_{\rm h}(t)$ rises and falls with kinetics at comparable time scales, in that $\tau_{\rm h}$ remains between 2.0 and 2.4s. The range of $m_{\rm h}$ values over one cycle period varies between approximately $(0.14, 0.53)$ and $(0.13, 0.59)$ as $\bar{g}_{\rm SynS}$ increases over the interval $[100, 300]$. The steady state activation $m_{\rm h,\infty}(V)$ reduces to zero almost entirely by $V = -0.04$ from its maximum near 1, occurring at the bottom of the actualized voltage range of a burst ($V \approx -0.06$). The consequence of this is that $m_{\rm h}$ will relax exponentially towards zero when $V > -0.04$, i.e., during spiking. Thus, B and I exhibit qualitatively distinct forms of $I_{\rm h}$ dynamics.

Normalized current data for one entire I state is shown in Figure 2 in a log-scale plot. These data are computed by normalizing all currents at time t to whichever is the greatest in magnitude, and separating the inward and outward currents for clarity. The largest current magnitude is therefore always represented by the value 1 (if inward) or -1 (if outward). Data for B is not shown because the normalized $\log_2(|I_{\rm h}|)$ at the beginning of B is smaller than $1/8$ and diverges below $1/16$ after only three spikes, so that we will consider $I_{\rm h}$ to play a minor role in this state, at most.

A subtle aspect of the mechanism of escape during I involves an interplay between the hyperpolarizing spike-mediated synaptic input ($I_{\rm SynS}$) that activates $m_{\rm h}$ and the depolarizing effect of $I_{\rm h}$ as it is increasingly activated. As is visible in Figure 3a, the inhibited neuron is most hyperpolarized near the beginning of I when the ISIs from the active neuron are shortest. Due to its long activation time constant, the hyperpolarization-activated $I_{\rm h}$ does not reach its maximum until the latter part of I. At this time, the ISIs between the synaptic input pulses have increased, and the membrane potential is depolarizing due to the resulting reduction in

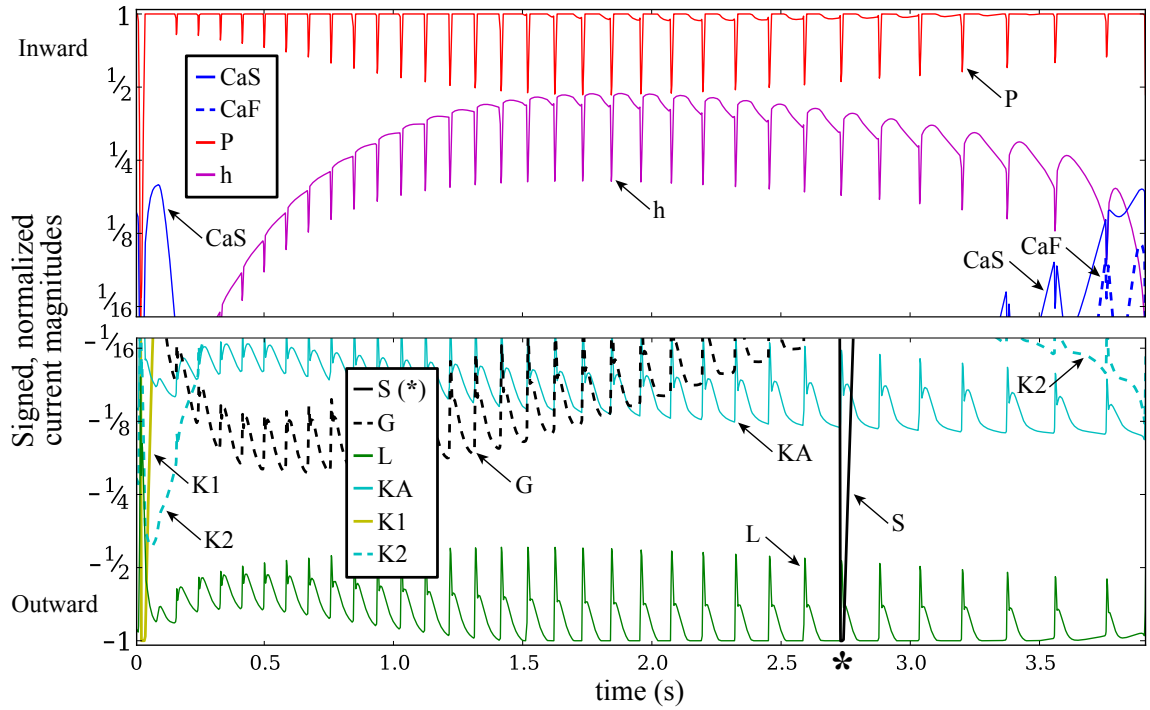

Fig. 2 Signed and normalized current magnitudes during the entire inhibited state of a single burst cycle at $\bar{g}_{\mathrm{SynS}} = 150$, shown in log scale as a fraction of the largest current (of either sign) at every time step. The positive scale shows inward currents, while the negative scale shows outward currents. For clarity, only one representative spike in the spike-mediated synaptic current I_{SynS} is shown at the instant marked with the asterisk. Nearly identical spikes are present at every other corresponding position in the plot, fitting in the sharp notches in the lines for the other currents, including a sole spike that does not become most dominant at $t \approx 0.1$s.

inhibition and the existing activation of I_{h}. Although the depolarization causes $m_{\mathrm{h},\infty}(V)$ to return towards 0, the long time constant of m_{h} means it does not immediately respond. Thus, I_{h} has an enhanced opportunity to depolarize the cell as it transitions to B because of the reduced inhibition. Indeed, as we discuss later, if the ISIs do not increase then the inhibited cell may never escape. Hill et al. demonstrated that the active neuron's ISIs must increase to a critical value in order to release the inhibited cell [14]. The primary change for I_{h} seen in Figure 2 near the end of I is the reduced driving force as the membrane potential increases towards E_{h}.

In the same work, Hill et al. also calculated that increasing $\bar{g}_{\mathrm{h}}$ in the model decreases the average ISIs in B [14]. In conjunction with the existence of a critical ISI for release of the inhibited neuron, this suggests that I_{h} might play a minor role in setting this critical value, and therefore participate in the mechanism for release as well as escape. Although the authors did not draw an explicit conclusion from these observations, we will directly address that role through Hypothesis 4, which is defined in the next section.

Figure 2 indicates that I_{P} and I_{L} are the largest currents for most of I. I_{P} slightly decreases over the first 0.5s and then remains almost constant in relative magnitude for the remainder of I. I_{CaF} only appears to be large enough to be involved in the dynamics within the final two arriving spikes of I in the transition to B. On average, I_{SynG} changes on a much slower time scale than action potential generation, and seems to play a secondary role at the beginning of I until I_{h} becomes large. I_{SynS} fluctuates at a fast time scale and creates the regular punctuations in the graph as it transiently dominates all other currents when it is active. For clarity in Figure 2, only one representative fluctuation due to a single action potential is shown. This transient effect of I_{SynS} on the other currents is due to the transient fluctuation in the membrane potential that it causes, which in turn briefly affects the driving force terms of those other currents.

I_{h} is small at the beginning of I but becomes one of the largest currents ($|I_{\mathrm{h}}| \sim |I_{\mathrm{P}}|/2$). Broadly speaking, I_{h} deactivates during B and activates during I, but its influence peaks in the middle of I, approximately $\sim$1s in advance of the onset of B for the canonical parameter values. We will explore whether this is important mechanistically, although it is already known from varying τ_{h} that the exact relative position of the peak in I is not crucial to the mechanism of transition to B [24].

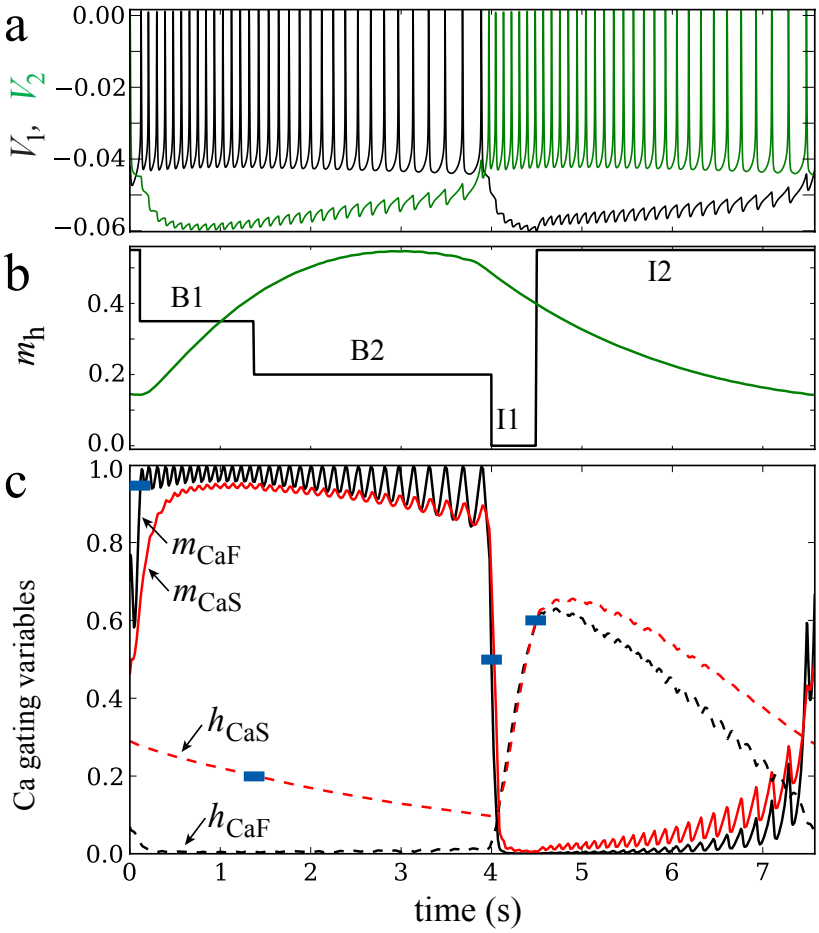

Fig. 3 The most relevant state variables over one oscillation period for the hybrid dynamical systems model $\mathscr{M}_R$ at the canonical $\bar{g}_{\text{SynS}} = 150$. a) Voltage traces ($V_1$ in black, bursting first, and V_2 in green). The sudden change in V_1 at $t \approx 4.5$s is due to the discrete change in vector field between I1 and I2 in neuron 1. b) m_h (neuron 1 in black, unreduced neuron 2 in green), with the four abstracted regimes labeled for neuron 1. c) Ca gating variables for neuron 1 only: m_{CaF} (solid black line), m_{CaS} (solid red), h_{CaF} (dashed black), h_{CaS} (dashed red), and thresholds used for defining m_h dynamics in Eq. (2) are shown by horizontal blue bars.

4 Hypotheses

We now formulate hypotheses from the above observations in the context of the five functional criteria for judging the existence and robustness of the bursting rhythm, and the control of the escape-release mechanism that transitions the system between bursting (B) and inhibited (I) states. The hypotheses allow us to propose answers to the general questions R1–R4 posed above, concerning the roles of I_h in the leech heartbeat HCO:

H1: I_h changes phasically over one cycle so that symmetry is maintained between the output of the two neurons (as they must generate symmetric and opposite driving activity to motor neurons on each side of the body).

H2: I_h is only important for the rhythm's existence towards the middle of I.

H3: I_h must be present (but small) immediately after I for robust initialization of B.

H4: I_h must be present (but small) later in B to ensure a slower increase of ISIs and prevent premature release of the other neuron.

H5: I_h does not need to be smoothly varying to function in the cell. While being a natural consequence of the underlying chemical kinetics, the functional requirements of I_h in the working of the cell can be represented using simpler terms (e.g., as a piecewise constant function).

H6: The working levels of I_h can be set according to an effectively discretized state of the system, not requiring precise or continual feedback from the membrane potential. In particular, four state-dependent

regimes are sufficient, B1, B2, I1, and I2—based on using the magnitude of calcium current to split B and I into two parts (of non-equal duration) each.

H7: The escape-release mechanism of the cycle can be reproduced by a reduced model of the HCO that satisfies H1–H6.

The final hypothesis, H7, is the largest in scope and builds from the previous hypotheses. It is presented more explicitly as a hybrid dynamical system.

4.1 A reduced hybrid dynamical systems model

We will test the above hypotheses by building a form of hybrid dynamical system model used in a previous analysis of a bursting neuron by Clewley et al. [5]. A hybrid dynamical system flexibly combines finite-state logic for simplified components with ordinary differential equations [26]. As illustrated in Figure 1, we choose to reduce the HCO model $\mathscr{M}_R$ using a piecewise constant dynamic process for the dynamics of m_h in neuron 1 only, and is otherwise defined in the same way as neuron 2, according to Section 2. We do not reduce both neurons in order to more strongly test the compatibility of the reduction in the context of the original circuit. A circuit where both neurons are reduced sustains bursting oscillations (not shown), but it is harder to be certain that artifactual mechanisms are not introduced or original mechanisms not lost when neither neuron possesses all the original model equations.

The above observations of temporal patterning in the current magnitudes over one cycle suggested four regimes for the reduced I_h. Major differences in the currents between B and I in this model have previously been identified for I_CaS and I_CaF [14], where they are large (small) in B (resp., I). A reduction using calcium thresholds to separate regimes for these states of a bursting neuron model was used in [5], and a similar approach is applicable here. For reference, the gating variables for I_CaS and I_CaF are shown over one cycle in Figure 3c. Two of the distinct regimes correspond to beginning the bursting and inhibited states of the cycle, which we will refer to as B1 and I1, respectively. The onset of B1 can be defined in several ways, but a robust choice is the crossing from below of a high threshold (0.96) on m_CaF. The onset of I1 will be defined as the crossing from above of a lower threshold (0.5) on m_CaF. The other two regimes correspond to the later parts of B and I, which we will refer to as B2 and I2 respectively. The transition to B2 is defined by the inactivation h_CaS falling through a threshold, which we chose to be 0.2. The transition to I2 is defined by h_CaF reaching a local maximum during this state. The four transition points are indicated in Figure 3c, but their exact positions are not crucial to the analysis that follows. We can now define the piecewise constant m_h in $\mathscr{M}_R$ as:

$$m_\mathrm{h}(t) = \begin{cases} m_\mathrm{h,B1} & \text{when in B1,} \\ m_\mathrm{h,B2} & \text{when in B2,} \\ m_\mathrm{h,I1} & \text{when in I1,} \\ m_\mathrm{h,I2} & \text{when in I2.} \end{cases} \tag{2}$$

The resulting set of states and transitions is summarized in Table 1, which will be referred to as the "template" of the bursting rhythm's mechanism (after [3]). As we focus on I_h only, the template does not exhaustively list all properties of the system in each state. The depolarized and hyperpolarized state conditions on the membrane potentials are not quantified in terms of voltage domains because there are no clear-cut voltage thresholds in the model that uniquely separate such domains. Instead, changes in the gating variables for I_CaS and I_CaF provide a more robust means to distinguish B from I. The template is an intermediate step in defining a hybrid dynamical system model that prepares us to test hypothesis H7.

The template describes a cycle for neuron 1, and requires an assumption that neuron 2 undergoes the same pattern of state changes (in anti-phase). Therefore, this is a recursive definition, and requires a self-consistency argument to validate it. As such, it is valuable to explicitly test the self-consistency through a simulation of a hybrid dynamical system. Here, we do not make use of the increasing of ISIs in B2 as a defining characteristic, although this would be an interesting direction in which to develop the model.

The values chosen here to define $\mathscr{M}_R$ are $m_\mathrm{h,B1} = 0.35$, $m_\mathrm{h,B2} = 0.2$, $m_\mathrm{h,I1} = 0$, and $m_\mathrm{h,I2} = 0.55$, which roughly mimic the rise and fall of m_h in $\mathscr{M}_F$. For these values, the HCO produced roughly symmetric anti-phase bursts at $\bar{g}_\mathrm{SynS} = 150$, a single cycle of which is shown in Figure 3 for some of the key variables. $m_\mathrm{h,I1}$ was set at zero instead of a value close to that seen in $\mathscr{M}_F$ in I1 (such as 0.15) in order to better test that I_h is only important for the rhythm's existence towards the middle of I (hypothesis H2).

Table 1 The template description of the escape-release mechanism hypothesis of bursting dynamics (H7) and the bursting rhythm relative to I_h in terms of states and their allowed transitions. The template is a summary of observations in Section 3 and hypotheses H2–H4 (Section 4) and is the basis of formally defining the hybrid dynamical system in Section 4.1. The first column indicates the discrete states of the hybrid dynamics, B1, B2, I1, I2, each separated by a row defining the transition between successive states. An upward (downward) arrow indicates an event threshold for the indicated gating variable for an increasing (resp., decreasing) transition. The asterisk for B2 indicates a recursive self-consistency assumption described in the main text.

State / Trans	Characterizing description	Role of I_h / transition in neuron 1
B1	Depolarized V_1 with regular spiking, hyperpolarized V_2	For robustness only (H3)
B1 $\rightarrow$ B2	Dominance of I_{CaS} reduces (ISIs begin to increase rapidly $\Rightarrow$ "release" of V_2)	$h_{CaS} \downarrow$
B2	Depolarized V_1 with regular spiking, hyperpolarized V_2	For modulation of ISIs only (H4)
B2 $\rightarrow$ I1	V_2 pro-actively begins spiking ("escape") *	$m_{CaF} \downarrow$
I1	Hyperpolarized V_1 with regular spiking in V_2	None
I1 $\rightarrow$ I2	V_1 becomes sufficiently polarized to de-inactivate I_{CaS} and I_{CaF}	$h_{CaF} \uparrow$
I2	Slowly depolarizing V_1 with V_2 regular spiking	Causes depolarizing trend (H2)
I2 $\rightarrow$ B1	V_1 begins spiking, I_{CaS} and I_{CaF} activate strongly	$m_{CaF} \uparrow$

4.2 Numerical methods and testing protocol

All ODEs in this study were solved using the adaptive time-step Radau integrator [13] using an absolute tolerance of 10^{-8} and a relative tolerance of 10^{-6}. This solver was accessed via an interface with PyDSTool [6], an open source software environment developed by the author for dynamical systems modeling. It provides a common set of compatible tools for model specification, simulation, and toolboxes for applications. PyDSTool supports simulations with state- or time-dependent events and so can simulate hybrid dynamical systems of the kind described above. Each threshold crossing needed for the mechanism template is defined as a zero-crossing "event function," detected to a tolerance of 10^{-4} with respect to function values. Full code used for this work is available at `http://www2.gsu.edu/~matrhc/HCO.html`.

In this work, we vary the parameter $\bar{g}_{SynS}$ and compare the functional metrics between stable bursting rhythms in models $\mathscr{M}_F$ and $\mathscr{M}_R$. In some test cases, we report a "failure" of the system to sustain a stable bursting rhythm. A 60s settle time was used to allow the system to approach a stable rhythm before making measurements. However, it was observed that a true limit cycle was not eventually approached by either model $\mathscr{M}_F$ or $\mathscr{M}_R$ (discussed further in Section 6).

The canonical value of $\bar{g}_{SynS}$ from the originally published model (Hill et al. [14]) is $\bar{g}_{SynS} = 150$, which was used as the starting point for developing the reduced model $\mathscr{M}_R$. In line with the physiological ranges discussed in [20], $\bar{g}_{SynS}$ was varied between 50 and 300. The significance to H1–H7 of the constant values used to define m_h will be explored through an informal sensitivity analysis. The primary constant of importance for m_h in Eq. (2) was expected to be $m_{h,I2}$, and is the only one that cannot be set to zero for bursting to continue over the range of $\bar{g}_{SynS}$ under the conditions tested below. In fact, when $m_{h,B1} = m_{h,B2} = m_{h,I1} = 0$, bursting typically occurs in the network as $\bar{g}_{SynS}$ is varied. As a result, these m_h parameters will henceforth be referred to as "secondary."

5 Results

5.1 Period, phase symmetry, and duty cycle

The period, phase symmetry, and duty cycle are fundamental measures of the temporal properties of a half-center oscillator's rhythm. We define the cycle period as $T_{av} = (T_1 + T_2)/2$, where T_1 (T_2) is the difference between two successive burst onsets in neuron 1 (resp., 2). The phase symmetry in a cycle was measured by the difference in the timing of onsets to B in each cell, normalized by T_{av}. Thus, a value of 0.5 indicates perfect symmetry between the onset of B in each cell as well as equal periods in their oscillation. The duty cycle was measured for neuron 1 as the proportion of the period T_1 spent in the bursting state.

Figure 4 compares these metrics for HCO cycles between models $\mathscr{M}_F$ and $\mathscr{M}_R$ at the canonical parameters of Hill et al. [14], as a function of $\bar{g}_{SynS}$. The trend in period is similar and the phase symmetry for $\mathscr{M}_R$ is, on average, within 2% of that for $\mathscr{M}_F$. The duty cycles are similar in magnitude but are consistently lower for $\mathscr{M}_F$ by no more than 2%. These results support H1, H5 and H6, as both the reduced and unreduced neurons behaved similarly when coupled together.

5.1.1 Sensitivity analysis of m_{h}

If all values are set equal in Eq. (2) so that $m_{\mathrm{h}} \equiv 0.45$, the trend in period is correct for $\bar{g}_{\mathrm{SynS}} \leq 225$ but offset by approximately +1s, while at larger $\bar{g}_{\mathrm{SynS}}$ neuron 1 remains disproportionately longer in B such that the period increases greatly. The phase symmetry decreases from 0.48 at $\bar{g}_{\mathrm{SynS}} = 100$ monotonically towards 0.1 as $\bar{g}_{\mathrm{SynS}} \to 300$, also reflecting that neuron 1's bursting state becomes much longer than that of its partner. The duty cycle increased almost linearly up to 0.85 as a function of $\bar{g}_{\mathrm{SynS}}$. (The functional consequence would be skewed timing and duration in the activation of motor neurons driven from this CPG circuit.) A bursting rhythm did not exist at $\bar{g}_{\mathrm{SynS}} = 300$ for these settings. These tests support hypothesis H1, that phasic changes in I_{h} are necessary for correct and symmetric activity. These results are also consistent with H5 and H6, as both the reduced and unreduced neurons behaved similarly when coupled together.

When $m_{\mathrm{h}} \equiv 0.45$, the maximum hyperpolarization of V_1 is much lower. This is due to the continued presence of I_{h} in I1 at a level much greater than is observed in Figure 2 over the first 1s. Consequently, the voltage-dependent de-inactivations of I_{CaS} and I_{CaF} are lessened.

Setting the secondary values $m_{\mathrm{h,B1}} = m_{\mathrm{h,B2}} = 0$ changed the period by less than 0.1s at each $\bar{g}_{\mathrm{SynS}}$, except that stable rhythms failed to exist for 3 of the 11 $\bar{g}_{\mathrm{SynS}}$ values tested. This alteration made no average change to the phase symmetry, and reduced the duty cycles to a value 0.5 ± 0.2 for all $\bar{g}_{\mathrm{SynS}}$ values except 50. These results are consistent with H2, in that I_{h} is less important during B. They also support H3 and H4, in that the presence of small amounts of I_{h} in B helps to maintain a robust rhythm. In every case of failure, neuron 1 enters B and fires one (sometimes two) action potential spikes. At this point, well-timed inhibitory spikes originating from the overlap with neuron 2 at the end of its bursting state lead to an immediate suppression of V_1 from further spiking in this cycle. Subsequently, neuron 1 returns to a state of low $I_{\mathrm{CaS}} + I_{\mathrm{CaF}}$, which had not yet fully activated. This situation is shown in Figure 5 for a failure at $\bar{g}_{\mathrm{SynS}} = 150$, where it is compared to the robust dynamics at the canonical parameters. Recall that the highest level of m_{CaS} de-inactivation is not reached until about 3 spikes into B on a normal cycle (Figure 3c). Thus, even though the cell is already depolarized enough to be spiking, the spiking state is fragile until I_{CaS} increases to its full level. In the meantime, this test reveals that if m_{h} activation is present early in B, it allows the cell to recruit I_{h} in response to inhibition during the overlap of B and I in the two neurons. Here, recruitment means that the hyperpolarizing effect of the inhibition from the other neuron increases the magnitude of the driving force in I_{h}, namely $V_1 - E_{\mathrm{h}}$, thereby generating a depolarizing, restorative effect on the B state without involving a significant change in m_{h} itself.

When only $m_{\mathrm{h,B2}} = 0$ was changed from the default values, there were no failures in stable rhythm generation at the 11 $\bar{g}_{\mathrm{SynS}}$ values tested. From these tests we conclude that the failures all involved the inhibited neuron failing to escape, and thus B was not robustly initialized in the absence of I_{h}. This supports H3, that I_{h} is necessary to provide this robustness in B1. While the metrics showed no significant change for $\bar{g}_{\mathrm{SynS}} \leq 175$, all showed close quantitative matching of the fluctuations in $\mathscr{M}_F$ for larger $\bar{g}_{\mathrm{SynS}}$. This suggests that the reduced model for I_{h} would require greater refinement to explore a detailed quantitative comparison with $\mathscr{M}_F$. When $m_{\mathrm{h,I1}}$ was increased from 0 to 0.2 the only significant change in these metrics was a small improvement in the agreement of period between $\mathscr{M}_F$ and $\mathscr{M}_R$ at $\bar{g}_{\mathrm{SynS}} \geq 175$.

5.2 Inter-spike intervals

Hill et al. describe how ISIs during a burst must increase to a critical value to release the other neuron from a suppressed state [14]. Here, we study the role of the different temporal components of I_{h} on ISIs in relation to this part of the rhythm's mechanism.

Figure 6 shows three representative sets of inter-spike intervals (ISIs) during the bursting state, as a function of spike number. In all cases, the last ISI of the burst was $\sim$0.22s. The number of spikes are similar between models $\mathscr{M}_F$ and $\mathscr{M}_R$, and the match in both value and slope is close except for a small step up in the values for $\mathscr{M}_F$ around spikes 12–20. These steps are due to the abrupt change in m_{h} between B1 and B2. Although quantitatively small, the difference in slope between $\mathscr{M}_F$ and $\mathscr{M}_R$ indicates a greater modulatory effect of I_{h} on inter-spike timing during B than was assumed from the normalized current magnitude values. Overall, these results support H1, H5 and H6, as both the reduced and unreduced neurons behaved similarly when coupled together. The exact number of spikes per burst occasionally varies by ± 1 on some cycles, due to the weakly chaotic nature of the attractor (see Discussion).

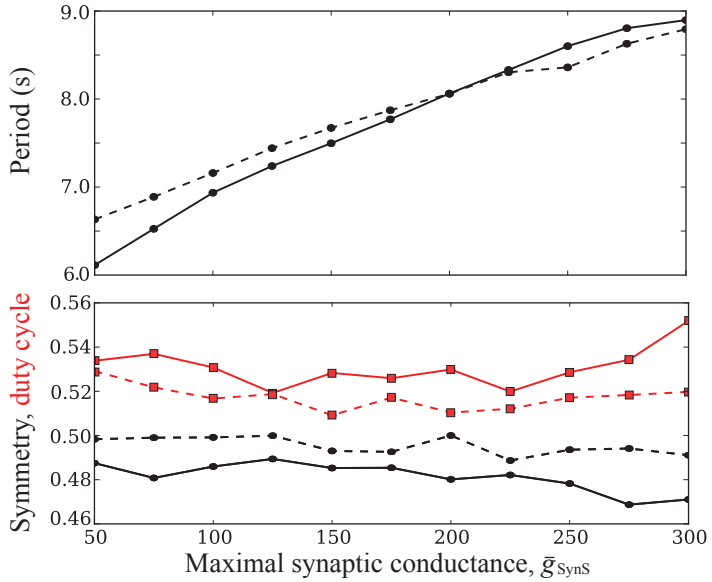

Fig. 4 Period, phase symmetry, and duty cycle metrics as a function of $\bar{g}_{\mathrm{SynS}}$. Solid lines: model $\mathscr{M}_R$. Dashed lines: model $\mathscr{M}_F$. In the lower panel, phase symmetry is shown in black with oval markers, and duty cycle is shown in red with square markers.

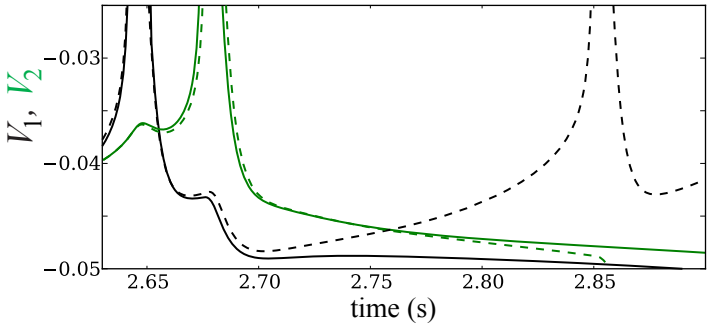

Fig. 5 Sensitivity to well-timed synaptic inputs at the end of the inhibited state. When $m_{\mathrm{h,B1}} = m_{\mathrm{h,B2}} = 0, \bar{g}_{\mathrm{SynS}} = 150$ in model $\mathscr{M}_R$, the (reduced) neuron 1 enters the B1 regime just before the first voltage spike (V_1 in black) as a result of $m_{\mathrm{h,B1}} = 0$. The solid lines show that V_1 is suppressed after interacting with the final spike of the bursting state in neuron 2 (V_2 in green). For comparison, the successful continuation of B for V_1 when $m_{\mathrm{h,B2}} = 0.2$ and $m_{\mathrm{h,B1}} = 0.35$ (their default values) is shown by the dashed lines.

5.2.1 Sensitivity analysis of m_{h}

Setting the secondary values $m_{\mathrm{h,B1}} = m_{\mathrm{h,B2}} = 0$ led to ISIs with the same increasing trend but a constant offset of between +0.01 and +0.02s for all $\bar{g}_{\mathrm{SynS}}$ values tested, with a greater discrepancy as spike numbers increase. This discrepancy increased the overall number of spikes per burst by up to 5. When only $m_{\mathrm{h,B2}} = 0$ the initial ISIs closely matched those shown in Figure 6, but after spike 20 the steeper upward trend persisted. The largest ISIs in these tests were all ∼0.22s. These results are consistent with H2, in that the fit between the ISIs of $\mathscr{M}_R$ and $\mathscr{M}_F$ is mostly due to the primary value $m_{\mathrm{h,I2}}$. The results also support H4, that the decline of I_{h} during B plays a role in controlling the increase of ISIs. As noted above, setting $m_{\mathrm{h}} \equiv 0.45$ led to longer bursting states in the reduced neuron with a smaller increase in ISI. In particular, for $\bar{g}_{\mathrm{SynS}} < 250$ the maximum ISI was no more than 0.03s smaller than that shown in Figure 6, but for larger $\bar{g}_{\mathrm{SynS}}$ neuron 1 entered a tonic spiking mode with constant ISIs sufficiently small to keep neuron 2 suppressed indefinitely. These results support the suggestion by Hill et al. that ISIs in neuron 2 must increase to a critical value (∼0.22s) in order to first release neuron 1 so that it may escape [14].

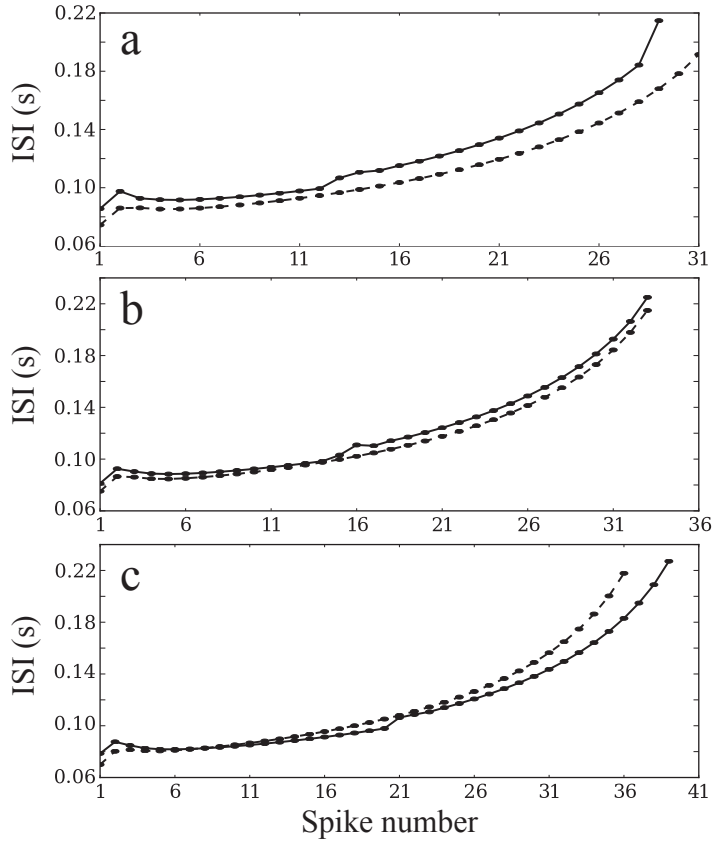

Fig. 6 Inter-spike intervals (ISIs) during the bursting state as a function of spike number within a burst, compared between models $\mathscr{M}_F$ (dashed lines) and $\mathscr{M}_R$ (solid lines). a) $\bar{g}_{\mathrm{SynS}} = 100$, b) $\bar{g}_{\mathrm{SynS}} = 200$, c) $\bar{g}_{\mathrm{SynS}} = 300$.

5.3 Response to perturbations

Under typical circumstances, a CPG should continue to function robustly in spite of mild perturbations to its state. "Perturbations" may arise in the form of small, noisy changes in synaptic timing or efficacy, or similar temporal variations in other parameters or state variables. In this section we consider the phasic dependence of this CPG to small perturbations in voltage only, and how this changes as we adjust the reduced representation of I_{h} in $\mathscr{M}_R$. Our aim is to determine whether I_{h} has a role in creating robustness by measuring the similarity in phase response between $\mathscr{M}_F$ and $\mathscr{M}_R$.

We consider the phase response of the circuit to weak current-pulse perturbations $I_{\mathrm{applied}}(t)$ applied to neuron 1, measured using the direct form of phase response curve (PRC) defined in [11]. The pulses were applied at spike-triggered times along the burst cycle, with a duration of 0.3s that is longer than any ISI within a burst. This minimizes artifactual differences between the models that arise from a sensitivity in response to the perturbation's precise timing relative to spikes [23]. Phase positions φ were selected at the next closest spike time to all spikes from the bursting state of neuron 1 when it was in B, otherwise from neuron 2 (making a total of 64–74 perturbations). Spike times were detected accurately during simulation using a voltage threshold of -0.02V.

The step pulse had amplitude 0.015pA, while its sign was negative (positive) for excitatory (resp., inhibitory) stimulation. The chosen amplitude was small enough so that inhibition at the canonical parameter values would not elicit catastrophic failure of B (transitioning to I) and excitation would not elicit immediate entry to B from I. (This would require additional transition rules in the mechanism template, e.g. for $\mathrm{B1} \to \mathrm{I1}$, and is beyond the scope of this work.) Thus, these perturbations are much weaker than those naturally made through synaptic coupling between the two neurons (as discussed in Section 5.1.1). The phase difference $\Delta\varphi$ on the next cycle (hereon denoted 1^{o} PRC) and the subsequent cycle (2^{o} PRC) in comparison to an unperturbed cycle was determined in the following way. The next onsets to B were measured accurately using burst

onset events in the simulations, and the difference between successive times to begin B were divided by the unperturbed cycle period. $\Delta\varphi < 0$ (> 0) indicates a delay (resp., advance) in the start of the next cycle.

Figs. 7–9 show three representative sets of data as $\bar{g}_{\mathrm{SynS}}$ was varied for $\mathscr{M}_R$. B1 begins at $\varphi = 0$, and the other transition phases of the other hybrid model are marked by small rectangles in the bottom panels of the figures. The PRCs indicate little sensitivity of the CPG for most phases except for φ in the ranges from 0.35–0.45 and 0.8–1.0, corresponding to the latter parts of the bursting or inhibited states. At most phases there is qualitative similarity in the responses of models $\mathscr{M}_F$ and $\mathscr{M}_R$ for all values of $\bar{g}_{\mathrm{SynS}}$, although $\mathscr{M}_R$ shows a much smoother response as φ varies. Particular local trends common to both models are indicated by red arrows in the figures. Generally, these results support H1, H5 and H6, as both the reduced and unreduced neurons responded similarly.

Although the stimulus occurs over a duration longer than any one ISI and averages some effects of the discrete step change in m_{h} between regimes in $\mathscr{M}_R$, there remains a marked accentuation in the primary phase responses of $\mathscr{M}_R$ for φ in the range from 0.35–0.45 for inhibitory perturbations and $\varphi > 0.8$ for excitatory perturbations. This includes some sign errors in the 1^{o} excitatory PRC of $\mathscr{M}_R$ compared to that of $\mathscr{M}_F$, although these are largely mitigated by the beginning of the second cycle (shown by the comparison of 2^{o} PRCs).

The discrepancy in 1^{o} PRCs decreases with increasing $\bar{g}_{\mathrm{SynS}}$, suggesting that synaptic inhibition can mask artifacts introduced in the process of reduction to $\mathscr{M}_R$. The decrease in discrepancy was measured by comparing local minima or maxima in the 1^{o} PRCs in the aforementioned ranges of φ. In the case of the excitatory PRCs, the local minima for $\varphi > 0.8$ were measured. As $\bar{g}_{\mathrm{SynS}}$ increased from 100, through 200, to 300, the difference in these local minima changed from 0.056, through 0.046, to 0.032, respectively. For the inhibitory PRCs, the sizes of the local minima immediately prior to the local maxima at $\varphi \approx 0.4$, and the sizes of those local maxima, were both compared. For the same three $\bar{g}_{\mathrm{SynS}}$ values in increasing order, the difference in the minimum and maximum positions given as pairs were (0.023, 0.049), (0.021, 0.044), and (0.001, 0.031), respectively.

A surprising observation from Figs. 7–9 is that there can be similar phase response effects in both models from both excitation and inhibition around certain phases, such as $\varphi \approx 0.4$ in both models and $\varphi \approx 0.9$ in $\mathscr{M}_F$. A preliminary examination of the number of spikes in the bursts of each neuron immediately following the perturbation provides some insight as to the reason. The 1^{o} PRC measures the proportional change in the perturbed cycle's duration compared to the unperturbed cycle. For this HCO, the increasing ISIs follow a typical pattern (Fig. 6), and so we expect a coarse correspondence between the temporal duration of the cycle and the total number of spikes per burst in the two neurons before the cycle repeats. Also, within the cycle including the perturbation, a change in the number of spikes per burst in each neuron of the pair provides more detailed temporal information about the circuit's response than the PRC.

For instance, we consider $\bar{g}_{\mathrm{SynS}} = 200$ and $\varphi = 0.4$, for which the unperturbed number of spikes per burst is 33. For the 1^{o} excitatory PRC, the number of spikes in the perturbed burst of neuron 1 was 35, and the number for the next burst of neuron 2 was 37. This is a total change of +6, resulting in $\Delta\varphi \approx 0.02$. For inhibition, the number of spikes in the corresponding bursts were 30 and 51, respectively, giving a total change of +15, resulting in $\Delta\varphi \approx 0.04$. Thus, in both cases the immediate response was intuitive: excitation led to a longer B while inhibition made it shorter. But in both cases there appears to be a longer-term compensatory mechanism that leads to a longer I after B is either shortened or lengthened, sufficient to create a longer overall cycle.

Similarly counter-intuitive phase-dependent effects of excitation and inhibition have been observed in isolated bursting neurons by Sherwood and Guckenheimer [23], which were analyzed using geometrical arguments based on a fast-slow decomposition [21]. In order to minimize such effects here, the phases at which perturbations were applied were chosen to correspond to the beginning of a spike. Nonetheless, ISIs increase during B so that the time at which a perturbation ends relative to a later spike is not consistent. Thus, the situation may be similar to that in [23], in that it involves small changes in perturbations relative to spike times, which alter the number of spikes during B, and hence cause a potentially large change in the duration of B (see Fig. 5 for a similar example). A full analysis of this situation would involve details of the fast sub-system for spike generation in addition to the longer-term compensatory effects in the other neuron. The time scale of spikes is faster than those considered in the present reduction, which does not isolate the spiking dynamics, and is beyond the scope of this work.

Additionally, the smoother response of $\mathscr{M}_R$ suggests that the detailed temporal dynamics of m_{h} activation contributes to the small fluctuations in $\Delta\varphi$ through small changes in the number of spikes per burst. From a quantitative perspective this may challenge the assumption that smoothness of I_{h} is unnecessary (H5), but the

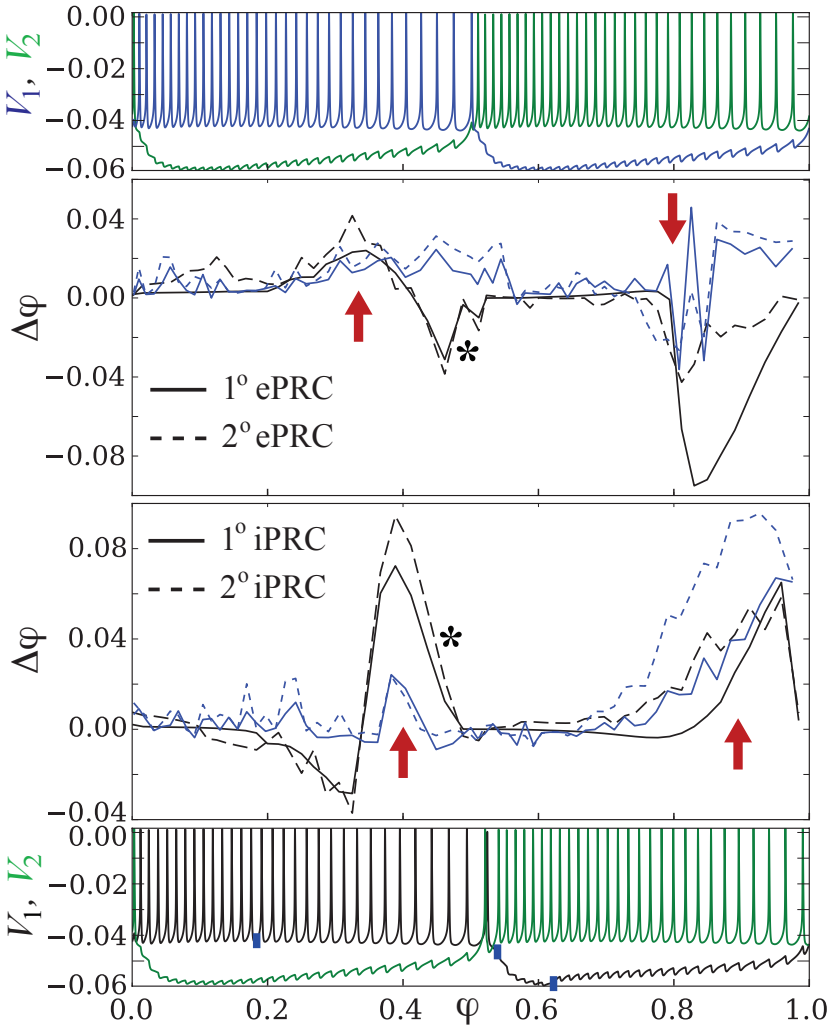

Fig. 7 Comparison of 1° and 2° excitatory (ePRC) and inhibitory (iPRC) phase response curves between models $\mathscr{M}_F$ (blue voltage traces and PRCs) and $\mathscr{M}_R$ (black voltage traces and PRCs) for $\bar{g}_{\text{SynS}} = 100$, as a function of the phase of step-pulse perturbation. All perturbation phases are spike-triggered (see main text for details). For reference, the top panel shows voltage traces for one full cycle of each neuron in the HCO of $\mathscr{M}_F$, and the bottom panel shows one full cycle for $\mathscr{M}_R$ (V_2 is always in green, bursting after neuron 1). V_1 always corresponds to the perturbed neuron, V_2 to the unperturbed neuron. Rectangular markers in the bottom panel indicate transition times between regimes for $\mathscr{M}_R$. Red arrows indicate positions of qualitatively similar trends in the responses. Secondary PRCs for $\mathscr{M}_R$ are shown with longer dashes, and both PRC traces for $\mathscr{M}_R$ are marked with an asterisk in a region where they are close to each other.

broader functional consequence of such a fine-grained and weak difference is unclear, and should be tested against more sophisticated metrics.

5.3.1 Sensitivity analysis of m_{h}

When the secondary values $m_{\text{h,B1}}$ and $m_{\text{h,B2}}$ were set to zero there were no differences in either the excitatory or inhibitory PRCs for $\bar{g}_{\text{SynS}} = 100$, 200, or 300 above the background level of fluctuation (± 0.02) seen in Figs. 7–9 for $\mathscr{M}_F$. Recall that in Section 5.1 we found that in this situation rhythms failed to exist for 3 of the 11 $\bar{g}_{\text{SynS}}$ values tested. However, as for those metrics, when the rhythms do exist, the lack of sensitivity we find for the PRCs here suggests no role for I_{h} in the robustness of rhythms to weak perturbations during B1 or B2. Increasing $m_{\text{h,I1}}$ from zero made no significant change to any of the PRCs.

The accentuated responses for $\varphi \approx 0.4$ in $\mathscr{M}_R$ involve neuron 1 receiving a perturbation during B2. Thus $m_{\text{h,B2}}$ was varied individually to explore whether modulation of I_{h} specifically around the time of perturbation

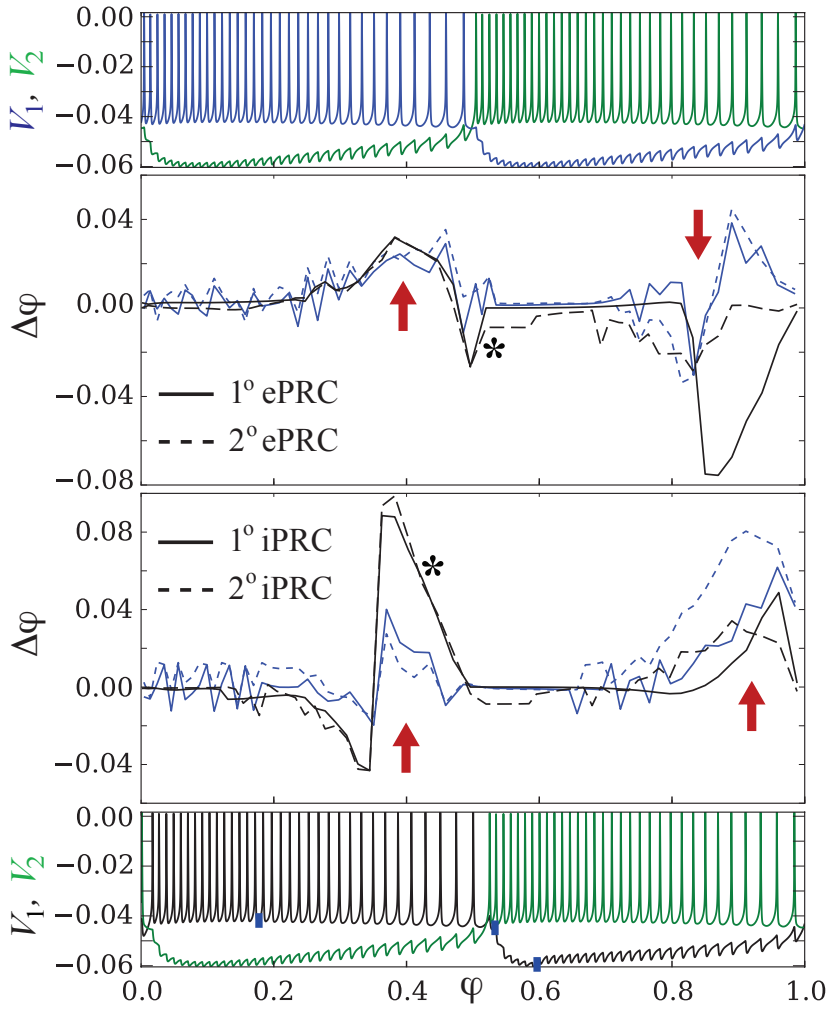

Fig. 8 Comparison of 1° and 2° excitatory and inhibitory PRCs between models $\mathscr{M}_F$ and $\mathscr{M}_R$ for $\bar{g}_{\mathrm{SynS}} = 200$. See legend for Figure 7.

could control the discrepancy in the phase responses. In particular, an increase in $m_{\mathrm{h,B2}}$ could be expected to decrease the ISIs during B2 and ensure greater domination of the bursting state by spiking currents so that perturbations would have less effect. However, setting $m_{\mathrm{h,B2}}$ to either 0.35 or 0 from the default value of 0.2 made no significant difference to the PRCs above the background level of fluctuation.

The accentuated responses for $\varphi > 0.8$ in $\mathscr{M}_R$ involve neuron 1 receiving a perturbation during I2. Thus $m_{\mathrm{h,I2}}$ was varied individually to explore this effect. Decreasing this value to 0.45 further accentuated the response by 2% for all $\bar{g}_{\mathrm{SynS}}$ values in the excitatory PRC (and also further accentuated the response at $\varphi \approx 0.45$ in the inhibitory PRC). At $\bar{g}_{\mathrm{SynS}} = 300$ an additional effect was a greater separation between the 1° and 2° PRCs of ~ 0.025. On the other hand, when $m_{\mathrm{h,I2}}$ was increased to 0.6 (which is close to the peak value for m_{h} for $\mathscr{M}_F$ at $\bar{g}_{\mathrm{SynS}} = 300$), the only significant change was uniformly greater separation between all the 1° and 2° PRCs by ~ 0.01.

We can conclude that the results of all the perturbation tests do not invalidate the hypotheses H1–H4 concerning the phasic nature of I_{h}, and that the PRC metric succeeds in demonstrating an important functional similarity of model $\mathscr{M}_R$ with $\mathscr{M}_F$. In addition, the results of the sensitivity tests lead us to conclude that there is no direct role of I_{h} at the time of perturbations arriving at the end of either B or I. Instead, we may expect a delayed connection between such perturbations and the dynamics that alter the next cycle's phase. In addition, the similarity between effects of excitation and inhibition at the end of B or I can be conjectured to involve different compensatory mechanisms between the coupled neurons that take place over an entire cycle period.

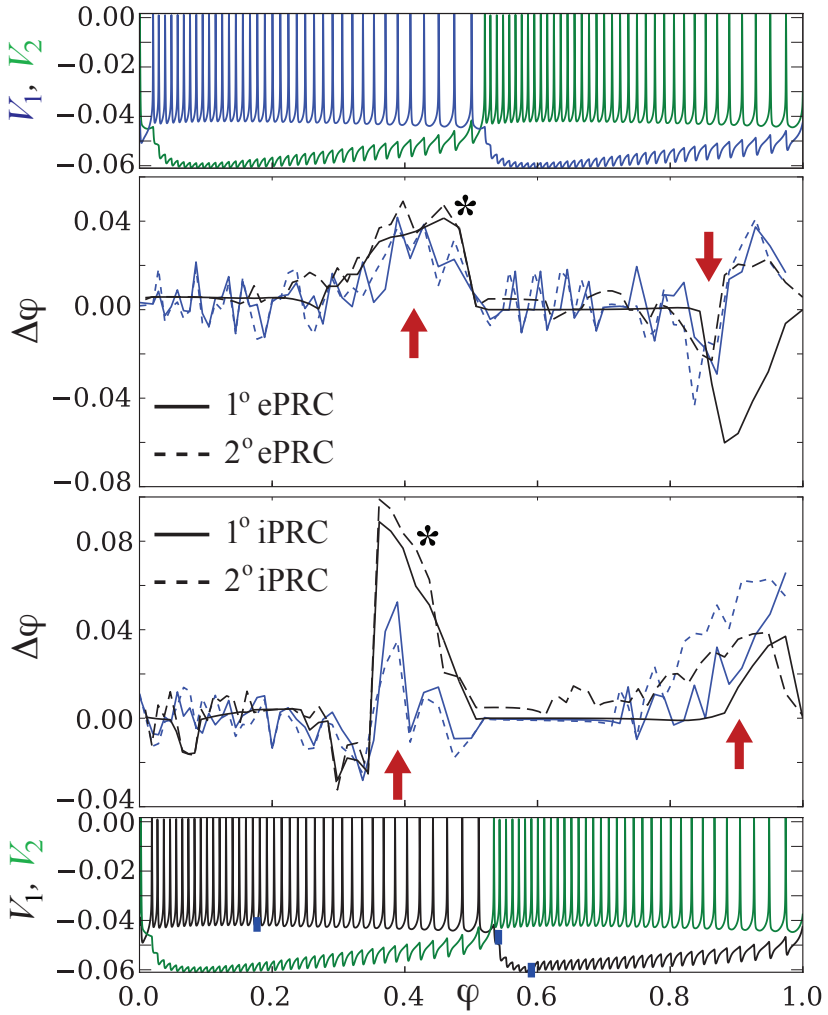

Fig. 9 Comparison of 1° and 2° excitatory and inhibitory PRCs between models $\mathscr{M}_F$ and $\mathscr{M}_R$ for $\bar{g}_{\text{SynS}} = 300$. See legend for Figure 7.

6 Discussion

In this work we formulated and tested simple hypotheses that elucidate the detailed role of the hyperpolarization-activated current I_h in creating functionally robust rhythms in a central pattern generator (CPG) model of the leech heartbeat. This model uses a half-center oscillator (HCO) architecture of two inhibitory interneurons. Previous investigations of this CPG through modeling studies (e.g., [14]) and experimental studies (e.g., [24]) have yielded possible mechanisms involving I_h in broad natural language terms. Here, our primary goal was to take advantage of an existing model and previous studies of its properties as an expository case study: we seek to validate the previous natural language descriptions through a more formal approach, and improve upon their clarity, robustness, and specificity. A secondary goal was to gain some fresh insights into the mechanisms involving I_h that were previously opaque.

6.1 Insight into the escape-release mechanism

To achieve our primary goal, we demonstrated a computational protocol for the hypothesis-driven testing of a formal description of the role of I_h in an "escape-release" mechanism. This used a reduction to a hybrid dynamical systems model. The tests were made with respect to five metrics that quantify essential aspects of rhythmic behavior, including the novel consideration of phase response of this circuit to mild perturbations.

These simple metrics are the most commonly used ones that relate to the functional properties of a CPG in an intact animal. Unfortunately, the precise connection between the metrics and broader functional properties are not yet well understood. Nonetheless, modification of some or all of the temporal properties measured by these metrics in an intact nervous system is a likely means of adapting and tuning rhythmic behavior. The resulting comparisons of our reduced and full models of the CPG were successful, and in the process we found results fully consistent with the conclusions of the previous studies, as well as new details and insights to the role of I_h. The new results are now discussed.

We established that only a transient step pulse of I_h is necessary during the inhibited state of a cycle to create a sustained bursting rhythm in the CPG and to dominate control of the cycle period. Only the broad timing of this pulse relative to the cycle phase is essential in this role, and not detailed temporal dynamics involving smooth activation and deactivation. We also established that the lower, "secondary" values of I_h present during its slow activation and deactivation elsewhere in the cycle do contribute some robustness to the rhythm. For instance, a residual amount of I_h appears to compensate for the incomplete activation of I_{CaS} at the beginning of bursting. This is helpful in providing robustness to the strong perturbations occurring when the bursting and inhibited states of the two neurons overlap.

The weak presence of I_h during the bursting state was shown to have an effect in modifying cycle period and spike-timing properties, although removing it in the later part of this state actually improved the fit of period, phase symmetry, and duty cycle to the full model.

Lastly, a stronger sensitivity of the phase response of the system to perturbations near the end of both the bursting and inhibited states was observed in both the full and reduced models. A surprisingly similar phase response from excitation and inhibition at some phases was also noted. The correspondence of these effects between the full and reduced models suggests that their functional significance could be investigated in future work using a reduced model of this kind along with additional metrics, such as the number of spikes per burst. Such an investigation is expected to require additional reductions at the fast time scale of spike generation to explore the interaction between disparate time scales. Both phase response effects could, for instance, be important for the correct modification of segmental phase by neighboring rhythmic segments in the ganglion under certain behavioral conditions.

In line with both the previous modeling studies of this CPG and more general analyses of asymmetric parameter changes in CPG circuits (e.g., by Daun et al. [9]), we find that changes in the parameters of one neuron affect the metrics for both neurons in a way that depends on the transition mechanism between the inhibited and bursting states of the collective rhythm. The escape-release mechanism discussed here is closest to the "neuronal adaptation" mechanism of transition discussed by Daun et al. in terms of globally-reduced phase-plane oscillator models [9].

On a technical note, it has been observed that the "regular" rhythms computed numerically for the original HCO model are close to limit cycles but do not appear to fully converge [8]. There is a lack of continued damping of variability in the period, ISIs, etc. of cycles as very long simulations are run, after an initial rapid damping from most initial conditions (within a few cycles). This occurs even at the highest integration tolerances and tightest step size control that resources allow, and suggests that the system may have a weakly chaotic attractor. The metrics computed for the model showed slight variability to the exact amount of settle time used to prepare the system, but the qualitative results and conclusions drawn are not sensitive to this. A mathematical study of the escape-release mechanism in its reduced form may elucidate the presence and nature of weak chaos in the model, and could be used to guide an optimization of parameters or equation structure in the dynamical system to seek a nearby regime in which the rhythmic solutions to the differential equations are limit cycles.

Although we only considered reducing a single current of one neuron's equations in one possible manner, our simple case study already demonstrates the value of our approach for future studies of complex neural dynamics. The process of analyzing dominant scales and reducing more of the current equations in similar ways can lead to substantially lower-dimensional representations of bursting dynamics [5]. Hybrid model reductions of five of the most dominant currents in the leech heartbeat HCO model are in progress, and preliminary results show stable and symmetric bursting oscillations when the reduced neuron is paired with an unreduced neuron. These reductions will permit testing of more sophisticated and fine-grained hypotheses about the relative roles of different currents in establishing and maintaining a bursting rhythm. However, rigorous computational protocols that test hypotheses involving many simultaneous reductions would be combinatorily complex, enough to require computer-aided management tools.

Our analysis protocol pinpointed where and how to further test the hypotheses, including how to introduce reasoning about additional currents and mechanisms. For example, the most important feedback loops

between the neurons in the escape-release mechanism occur at the end of the bursting and inhibited states of the two neurons, and are hypothesized to involve: *(1)* increases in ISI in the bursting neuron 2 (largely connected to inactivation of I_{CaS} but with a modulatory role for I_{h} suggested by Section 5.2.1), and *(2)* the activation of I_{CaS} and I_{CaF} as the inhibited state transitions to the bursting state in neuron 1, with a secondary role for a residual amount of I_{h} (Section 5.1.1). A functionally-driven reduction of all currents involved in this feedback could be expected to allow meaningful quantification of the *degree* to which release plays a role in comparison to escape. It may also facilitate phase plane and bifurcation analysis of the hybrid dynamics for these feedback loops, for instance along the lines of [2,3,5,7,9].

6.2 Towards formal, hypothesis-driven modeling

The formalized description of the escape-release mechanism took the form of a "template" that categorizes gross functional states of the system and indicates characteristic transitions between them [3]. A template is more explicit about its assumptions than a natural language description, and provides a clearer means to distinguish causal connections from correlations in the changing activity between the model's components. In particular, it increases analytical access to the effectively low-dimensional, transient regimes hypothesized from the full dynamics. We showed how a template can be represented as a hybrid dynamical system that encodes the causal hypotheses. The simulation of such a system directly tested that it is logically self-consistent and enables quantification of its success in mimicking the full model. Thus, we conclude that hypotheses H1–H6 could not be rejected by the tests presented here, so that H7 is supported: namely, the escape-release mechanism can be reproduced by the hybrid dynamical model, up to the resolution provided by our metrics.

This work argues that formalizing a mechanistic description in this way can increase its predictive power and facilitate greater parsimony, leading to a more precise understanding of biological function. This is important as the goals of large-scale, detailed computational modeling in neuroscience become more ambitious [15,17] at a rate that currently dwarfs the scope of mathematically-based theoretical tools. At present, large models are simulated with limited understanding of the roles that the thousands of parameters and connections play in the essential dynamic mechanisms underlying the observable properties of the system. Furthermore, some of these mechanisms may remain unidentified during simulation, and clear criteria for measuring the functional success of a large-scale model are extremely challenging to establish. A new generation of integrated informatic tools must tackle this situation and provide an explicit basis for judging when elements of model activity are (for example) biologically necessary, plausible, or artifactual. Such tools have not yet been synthesized, but in principle are within the reach of modern computer hardware, simulation tools, database tools, and qualitative reasoning algorithms. The present work demonstrates a prototypical technique in the spirit of envisioning how future informatic tools might work.

Acknowledgements The author would like to thank R. Lin and the anonymous reviewers for their helpful input.

References

1. Bongard, J., Lipson, H.: Automated reverse engineering of nonlinear dynamical systems. Proc. Nat. Acad. Sci. USA **104**(24), 9943–9948 (2007)
2. Channell, P., Cymbalyuk, G., Shilnikov, A.: Origin of bursting through homoclinic spike adding in a neuron model. Phys. Rev. Lett. **98**(13), 134,101 (2007)
3. Clewley, R.: Encoding the fine-structured mechanism of action potential dynamics with qualitative motifs. J. Comput. Neurosci. (e-pub ahead of print 18 August 2010) (2010)
4. Clewley, R., Rotstein, H.G., Kopell, N.: A computational tool for the reduction of nonlinear ODE systems possessing multiple scales. Multiscale Modeling and Simulation **4**(3), 732–759 (2005)
5. Clewley, R., Soto-Treviño, C., Nadim, F.: Dominant ionic mechanisms explored in the transition between spiking and bursting using local low-dimensional reductions of a biophysically realistic model neuron. J. Comput. Neurosci. **26**(1), 75–90 (2009)
6. Clewley, R.H., Sherwood, W.E., LaMar, M.D., Guckenheimer, J.M.: PyDSTool, a software environment for dynamical systems modeling (2007). URL `http://pydstool.sourceforge.net`
7. Coombes, S., Bressloff, P.C. (eds.): Bursting: The Genesis of Rhythm in the Nervous System. World Scientific (2005)
8. Cymbalyuk, G., Gaudry, Q., Masino, M.A., Calabrese, R.L.: Bursting in leech heart interneurons: cell-autonomous and network-based mechanisms. J Neuroscience **22**, 10,580–10,592 (2002)
9. Daun, S., Rubin, J.E., Rybak, I.A.: Control of oscillation periods and phase durations in half-center central pattern generators: a comparative mechanistic analysis. J Comput Neurosci **27**, 3–36 (2009)
10. Ermentrout, G.B., Terman, D.H.: Mathematical Foundations of Neuroscience. Springer (2010)

11. Govaerts, W., Sautois, B.: Computation of the phase response curve: A direct numerical approach. Neural Computation **18**, 817–847 (2006)
12. Grillner, S.: Control of locomotion in bipeds, tetrapods and fish. In: V. Brooks (ed.) Handbook of Physiology. Sec 1: The Nervous System. Vol. II: Motor Control, pp. 1179–1236. American Physiological Society (1981)
13. Hairer, E., Wanner, G.: Solving ordinary differential equations II: Stiff and Differential-Algebraic Equations, 2nd edn. Springer (1996)
14. Hill, A.A.V., Lu, J., Masino, M.A., Olsen, Ø.H., Calabrese, R.L.: A model of a segmental oscillator in the leech heartbeat neuronal network. J. Comput. Neurosci. **10**, 281–302 (2001)
15. Izhikevich, E.M., Edelman, G.M.: Large-scale model of mammalian thalamocortical systems. Proc. Natl. Acad. Sci. USA **105**, 3593–3598 (2008)
16. Marder, E., Calabrese, R.L.: Principles of rhythmic motor pattern generation. Physiol. Rev. **76**, 687–717 (1996)
17. Markram, H.: The Blue Brain project. Nature Reviews Neuroscience **7**, 153–160 (2006)
18. Nadim, F., Olsen, Ø.H., de Schutter, E., Calabrese, R.L.: Modeling the leech heartbeat elemental oscillator I. interactions of intrinsic and synaptic currents. J. Comput. Neurosci. **2**, 215–235 (1995)
19. Olypher, A., Cymbalyuk, G., Calabrese, R.L.: Hybrid systems analysis of the control of burst duration by low-voltage-activated calcium current in leech heart interneurons. J Neurophysiol **96**, 2857–286 (2006)
20. Olypher, A.V., Calabrese, R.L.: How does maintenance of network activity depend on endogenous dynamics of isolated neurons? Neural Computation **21**, 1665–1682 (2009)
21. Rubin, J., Terman, D.: Geometric singular perturbation analysis of neuronal dynamics. In: B. Fiedler (ed.) Handbook of Dynamical Systems, vol. 2. Elsevier (2002)
22. Shelley, M., McLaughlin, D., Shapley, R., Wielaard, J.: States of high conductance in a large-scale model of the visual cortex. Journal of Computational Neuroscience **13**, 93–109 (2002)
23. Sherwood, W.E., Guckenheimer, J.: Dissecting the phase response of a model bursting neuron. SIAM J. Appl. Dyn. Syst. **9**(3), 659–703 (2010)
24. Sorensen, M., DeWeerth, S., Cymbalyuk, G., Calabrese, R.L.: Using a hybrid neural system to reveal regulation of neuronal network activity by an intrinsic current. J Neuroscience **24**, 5427–5438 (2004)
25. Tobin, A.E., Calabrese, R.L.: Endogenous and half-center bursting in morphologically inspired models of leech heart interneurons. J Neurophysiol **96**, 2089–2106 (2006)
26. Van Der Schaft, A., Schumacher, J.M.: An Introduction to Hybrid Systems. Springer-Verlag, London (2000)